Desalination and Water Treatment
www.deswater.com

doi:10.5004/dwt.2019.23419

142 (2019) 244–251
February

Removal of iron (II) from wastewater in oil field using 3-(*p*-methyl) phenyl-5-thionyl-1,2,4-triazoline assembled on silver nanoparticles

Eid M.S. Azzam[a,*], Sayed A. Ahmed[b], Hussein H. Mohamed[b], Mohamed A. Adly[b], Elshafie A.M. Gad[a]

[a]*Applied Surfactants Laboratory, Petrochemicals Department, Egyptian Petroleum Research Institute, Nasr City, 11727 Cairo, Egypt, Tel. +20 1117710207; emails: eazzamep@yahoo.com (E.M.S. Azzam), eamgad_99@hotmail.com (E.A.M. Gad)*
[b]*Department of Chemistry, Faculty of Science, Beni-Suef University, 62514 Beni-Suef City, Egypt, emails: skader_70@yahoo.com (S.A. Ahmed), h_gendy_2010@yahoo.com (H.H. Mohamed), Mohamed.Atia@khalda-eg.com (M.A. Adly)*

Received 30 March 2018; Accepted 2 November 2018

ABSTRACT

In this work, we prepared 3-(*p*-methyl) phenyl-5-thionyl-1,2,4-triazoline (C1). The nanostructure of the prepared C1 compound was fabricated by assembling on silver nanoparticles (AgNPs). The ultraviolet and transmission electron microscope analyses confirm the assembling of the C1 compound on AgNPs. The effects of the C1 compound on the removal of iron (II) from iron-contaminated samples (prepared in the laboratory) and industrial wastewater samples (produced water from oil processing facility) were studied before and after their assembling on AgNPs. The removal of iron was studied at different concentrations of $FeSO_4$ solution (5, 14, and 39 mg/L), and field sample concentration was 661 mg/L. In addition, the removal of iron (II) was investigated at different times. The prepared compound shows high efficiency in removing the iron ions from the used water samples. The AgNPs have a good role in enhancing the removal of iron ions from the water samples. Quantum chemical descriptors using density function theory with the nonlocal correlation functional B3LYP with 6-311G ++ (p,d) basis set implemented in Gaussian 09 program were E_{HOMO} and E_{LUMO}. The output of the study pronounces that the C1 molecule can act as a chelating agent for iron (II).

Keywords: Triazole derivatives; Silver nanoparticles; Iron (II); DFT; Oil field

1. Introduction

Organosulfur compounds are a very important class of organic compounds and are widely used in the field of medicine for the treatment of various diseases such as cancer [1], antimicrobial diseases [2], etc. The naturally occurring organosulfur compounds, such as in garlic, have been verified to be antiviral [3], and it was reported that garlic is a strong antioxidant due to high levels of organosulfur compounds [4,5]. A very important group of organosulfur compounds, the thiols, have many biological activities as well as many industrial applications, and some thiols have good antimicrobial activities like bismuth thiols [6]. Thiol compounds have been widely used in the equipment used for the detection of flammable gas leaks like ethyl mercaptan, *sec*-butyl mercaptan, *tert*-butyl mercaptan, N-propyl mercaptan, and isopropyl mercaptan [7]. Recently, thiol compounds have been used in the removal of heavy metals like Cd, Pb, and Cu from water. The thiol-functionalized Fe_3O_4 at metal-organic core-shell microsphere possesses a highly selective removal of Pb^{+2} and Hg^{+2} ions from mixed metal ion wastewater [8]. Triazoles and its derivatives are a very important class of heterocyclic compounds. Triazole derivatives are biologically active compounds [9–14], corrosion inhibitors [15], dyes [16], acid-base indicators [17], and other industrial chemicals [18]. Recently, triazoles were used in

* Corresponding author.

1944-3994/1944-3986 © 2019 Desalination Publications. All rights reserved.

the removal of heavy metals, where new copolymers with triazole pendant groups were synthesized and applied for the removal of heavy metals, and the copolymer containing triazole rings with galactose residue showed good results as a resin for the cleaning of water contaminated with mercury [19]. Silver nanoparticles (AgNPs) are of interest because of their unique properties, the size, and shape depending on the optical, electrical, and magnetic properties. AgNPs have drawn the attention of researchers because of their extensive applications in areas such as integrated circuits [20], sensors, and filters [21]. Our approach in this work is the use of the synthesized 3-(*p*-methyl) phenyl-5-thionyl-1,2,4-triazoline (C1) and its nanostructure with AgNPs in the removal of iron (II) ions from wastewater in the oil field.

2. Materials and experimental techniques

2.1. Materials

2.1.1. Synthesis of p-methyl benzaldehyde thiosemicarbazone

This compound was prepared as shown in Fig. 1 by reacting *para*-methyl benzaldehyde (10 g, 0.1 mol/L) (98%, SCHUCHARD, Germany) with thiosemicarbazide (7.3 g, 0.1 mol/L) (98%, LOBA CHEMIE, India) in 50 mL ethyl alcohol (98%, BIOCHEM, Egypt) and refluxed for 6 h. The solvent of crystallization was ethyl alcohol, and the yield was white crystals. The melting point of this compound was 160–165 [22].

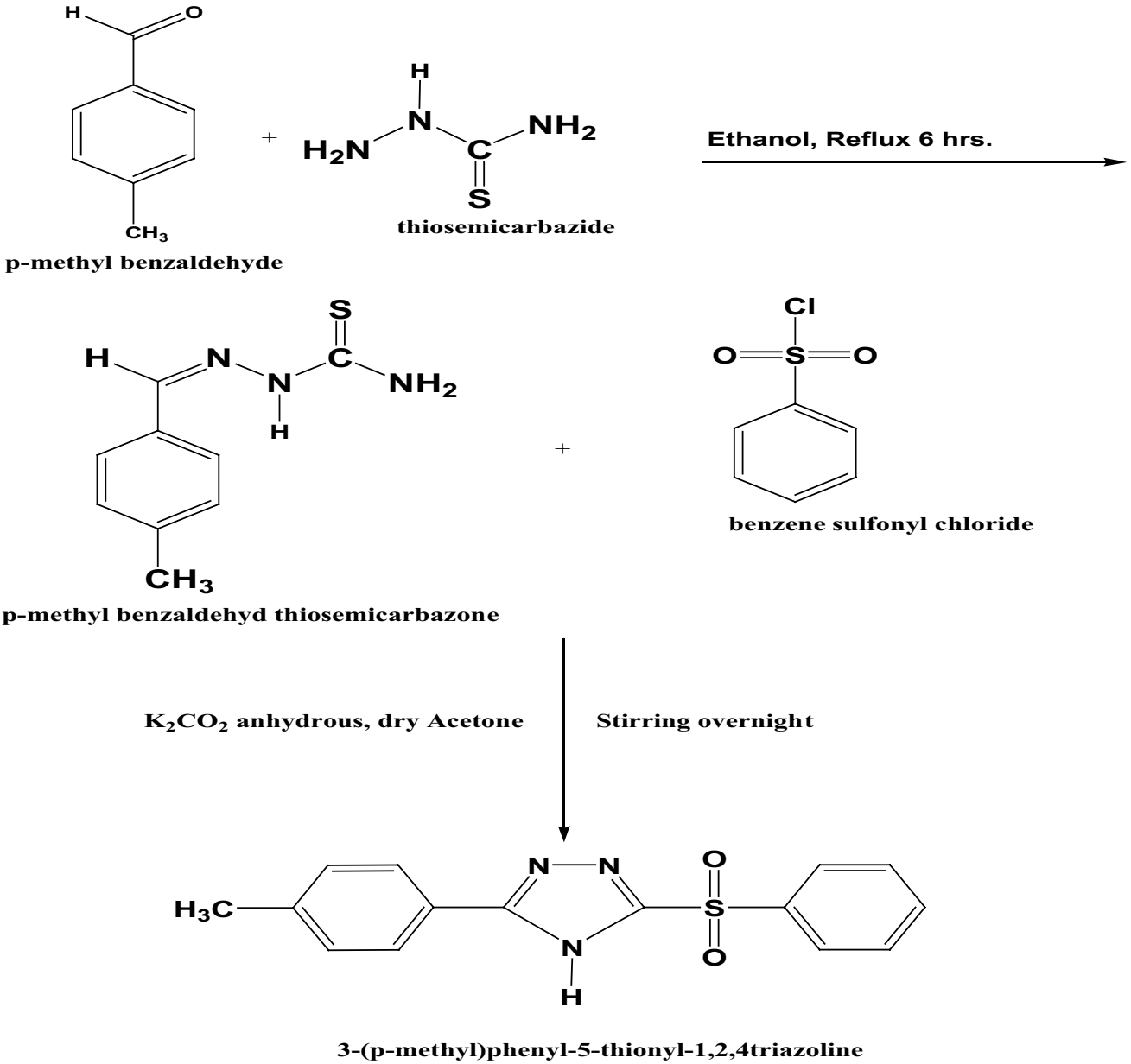

Fig. 1. Preparation of 3-(p-methyl) phenyl-5-thionyl-1,2,4-triazoline "C1".

2.1.2. Synthesis of C1

C1 compound was prepared by reacting *p*-methyl benzaldehyde thiosemicarbazone prepared in step 2.1.1. (5 g, 0.1 mol/L) with benzenesulfonyl chloride (4.5 ml, 0.1 mol/L) each in the presence of potassium carbonate anhydrous (3.5 g, 0.1 mol/L) in 10 mL dry acetone (98%) and stirring for 24 h then pouring over ice, filtration and crystallization from ethyl alcohol and gently dropping water. Melting points were 95°C–100°C, and the yield was yellow crystals (Fig. 1) [23,24].

2.1.3. Synthesis of the AgNPs

The AgNP colloidal solution was synthesized from silver nitrate using the chemical reduction method as shown previously [25]. $AgNO_3$ solution (100 ml, 1×10^{-3}M) in the conical flask was heated to boiling. Then 10 mL of 1% trisodium citrate was added drop by drop to silver nitrate solution. After stirring and heating, the solution was turned to the yellow color. The heating was stopped, and the mixed solution was stirred until cooled to room temperature.

2.1.4. Assembling of the poly(2-aminothiophenol) on AgNPs

The assembling of the synthesized C1 on AgNPs was carried out as follows: The AgNP solution (20 ml) was mixed with 5 mL solution of the C1 compound in dimethylformamide (0.1M). The mixture was stirred continuously for 24 h till the color change [26].

2.1.5. Preparation of the heavy metal solutions

In this work, depending on two ways for obtaining iron (II) solution, one is the practical method of preparing different concentrations (0.05, 0.15, and 0.5 mol/L) of iron (II) sulfate solution. The other way obtained a field sample from the drain of a separator of the crude oil processing facility located at Khalda petroleum company, Egypt, which contains a very high concentration of iron (II). Each sample was detected for determination of iron (II) concentration using DR5000 apparatus at wavelength 510 nm.

2.1.6. Removal of iron (II) from the prepared $FeSO_4$ solutions and field samples using C1

In this step, 2 mL of the solution of compound C1 (0.1M) was added to 20 mL of each ferrous sulfate concentration (0.05, 0.15, and 0.5 mol/L). Also, 2 mL of C1compound solution was added to the field sample. All samples were stirred for different periods (30 min, 3 h, and overnight). Each sample was detected for determination of iron (II) concentration using DR5000 apparatus after each period.

2.1.7. Removal of iron (II) from the prepared $FeSO_4$ solutions and an oil field sample using C1 compound assembled on AgNPs

In this step, 4 mL of the solution of compound C1 (0.1 M) assembling on AgNPs was added to 20 mL of each of ferrous sulfate concentration (0.05, 0.15, and 0.5 mol/L). Also, 2 mL of C1 compound assembled on AgNPs was added to the field sample. All samples were stirred for different periods (30 min, 3 h, and overnight). Each sample was detected for determination of iron (II) concentration using DR5000 apparatus after each period.

3. Experimental techniques

3.1. Infrared spectrometer

The Fourier-transform infrared spectroscopy (FTIR), 1HNMR and Mass spectrum are represented in Figs. S1–S3. All spectra were recorded with 2 cm^{-1} resolution at an angle of incidence 80° relative to the surface normal using a BSU_MIR_ATR.xpm spectrophotometer.

3.2. Proton nuclear magnetic resonance

Proton nuclear magnetic resonance (^{1}HNMR) measurements were performed on a BRUKER instrument

3.3. Atomic mass spectrometer

Mass measurements were done using mass spectrometer MSD 5975, using ion source/electron impact, its scale 50–1,200 g/mol.

3.4. Ultraviolet absorption measurements

The ultraviolet (UV) measurements were carried out by UV-2600Series photometer.

3.5. Transmission electron microscope

The transmission electron microscope (TEM) was measured as follows: Small droplets of the AgNP solution or the synthesized C1 compound with AgNPs were placed on the carbon-coated grid. A photographic plate of the TEM (Type JEOL JEM-1230 operating at 120 KV attached to a CCD camera) was employed on the present work to investigate the nanostructure of the prepared samples.

3.6. Detection of iron (II) concentrations

The detection of iron (II) was carried out using DR5000 UV-Vis spectrophotometer, HACH Company, Germany. Only 2 mL of the stirred sample was added to 100 mL of deionized water and then shaking it to reach a proper mixing. A 10 mL of the diluted sample was filled in each of two covets of DR5000; the indicator was put in one of them and mixed. The covet free of the indicator was used for zeroing the apparatus, then taking the reading of the other one, and then multiplying its reading by 100 due to the previous dilution. The dilution was made to match the scale of the apparatus.

4. Results and discussion

4.1. Chemical structure confirmation of the synthesized compounds

FTIR of the synthesized *p*-methyl benzaldehyde thiosemicarbazone shows NH symmetric and asymmetric stretches at 3,383.917 cm^{-1} and 3,232.532 cm^{-1}, aromatic CH stretch at 3,016.677 cm^{-1}, C=C three stretching bands at 1,593.719,

1,496.285, and 1,463.746 cm^{-1}, NH bending at 1,531.1994 cm^{-1}, CH bend for ρ-substitution at 824.78 cm^{-1}, and C-S stretching at 623 cm^{-1}. ^{1}HNMR spectra show peaks at s = 7.2–7.9 (m, 4H, aromatic), 8 (s, 2H, NH_2), 8.2 (s, 1H, CH=N), and 11.4 (s, 1H, NH). Besides, the mass spectra show peaks at *m*/*z* 197, 180, 122, 95, and 76. The FTIR for the synthesized C1 shows peaks of N-H stretch at 3,366.954 cm^{-1}, CH aromatic stretching at 3,089.894 cm^{-1}, C=C aromatic stretching showed three bands at 14,550.62, 1,518.141, and 1,573.024 cm^{-1}, N–H bend at 1,606.493 cm^{-1}, and S=O at 1,082.348 cm^{-1}. The ^{1}HNMR of C1 shows peaks at s = 1.2 (s, 3H, CH_3), 7.2–7.8 (m, 4H, aromatic), 7.9–8.2 (m, 5H, aromatic), 8.3 (s, 1H, NH), and 8.4 (s, 1H, NH). The mass spectrum of the C1 compound shows peaks at *m*/*z* 299, 158, 118, and 77. The mechanism of fragmentation is shown in Fig. 2.

4.2. Assembling of C1 on AgNPs

The assembling of C1 on AgNPs in this work was investigated using UV as shown in Fig. 1 and TEM as shown in Fig. 3. The UV in Fig. 4 shows the AgNPs peak at λ_{max} 433 nm. After assembling of the synthesized C1 on colloidal AgNPs, the peak at λ_{max} 433 nm was faded and other peaks appear at λ_{max} 277, 338 nm related to σ-σ * transition (E2-band) of benzene ring π–π* transition and B-band (A1g-B2u), which confirm the assembling of C1 molecules on the AgNPs.

Fig. 4 shows the TEM images of AgNPs before and after assembling of the prepared C1 compound. The prepared AgNPs are aggregate spherical particles, and the size of most of the silver particles is about 16–18 nm. After assembling of the synthesized C1, the AgNPs show smaller particle diameter about 18–21 nm. These particles are more dispersed and less aggregate than the individual AgNPs. The TEM images in Fig. 5 further revealed the stabilization of AgNPs due to interaction with the molecules of the synthesized C1 compound.

4.3. Removal of iron (II) from the prepared $FeSO_4$ solutions

We investigated the removal of Fe^{2+} from the $FeSO_4$ solutions (0.05M, 0.15M, and 0.5M) using the synthesized C1 compound individually and assembled on AgNPs (0.1M) at different times as shown in Table 1 and Fig. 5. The results in Table 1 and Fig. 5 show the activity of the synthesized C1 compound and its nanostructure with AgNPs toward the removal of Fe^{2+} from the solution which may be related to the covalent bond formation between the lone pair electron of nitrogen atoms and the positive charge of Fe^{2+} ions. It was noticed from the results in Table 1 and Fig. 5 that the concentration of Fe^{2+} decreases as the time increases from 30 min to overnight. In addition, the results in Table 1 and Fig. 3 indicate

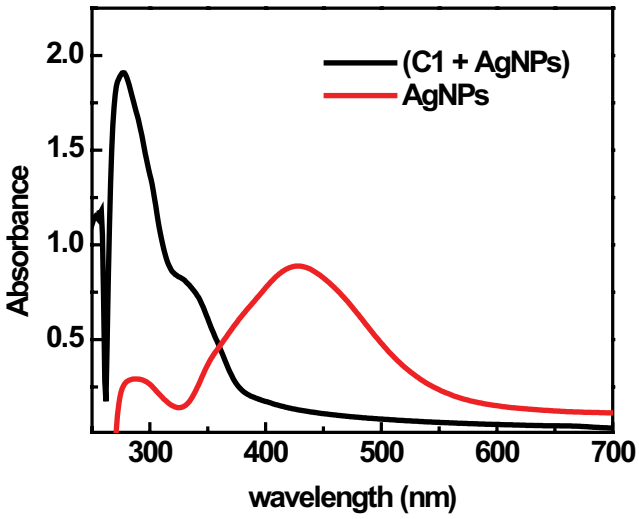

Fig. 3. UV spectrum of AgNP and C1 compounds assembling on AgNPs.

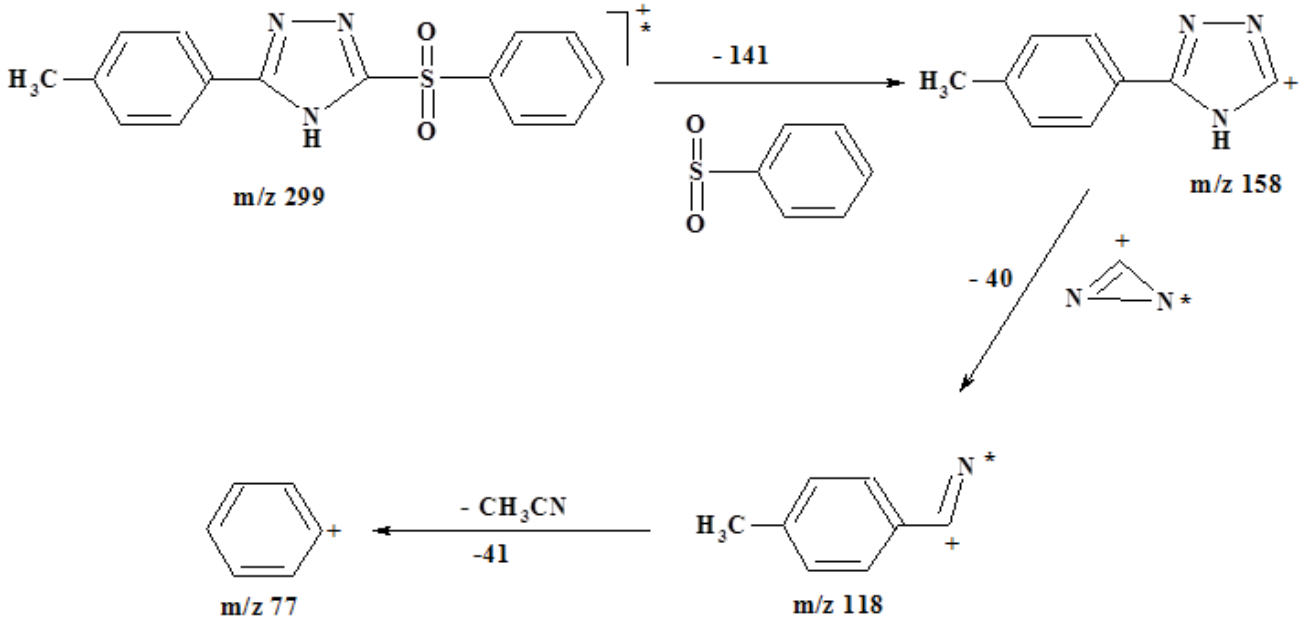

Fig. 2. Fragmentation mechanism of the synthesized C1 compound.

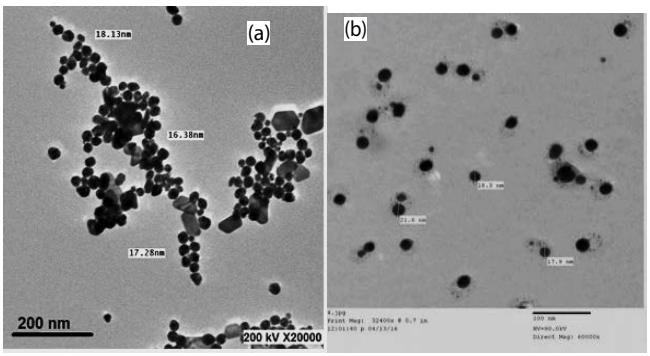

Fig. 4. TEM of AgNPs (a) and C1 compounds assembled on AgNPs (b).

Table 1
Removal of iron (II) from prepared $FeSO_4$ solutions using C1 compound individual and assembling on AgNPs

$FeSo_4$ solutions	0.05 M	0.15 M	0.5 M
Fe^{2+} concentration in blank solution	5 mg/L	14 mg/L	39 mg/L
Fe^{2+} concentration after addition of compound C1 (0.1 M)	**After 30 min**		
	1 mg/L	9 mg/L	34 mg/L
	After 3 h		
	1 mg/L	8 mg/L	32 mg/L
	Overnight		
	1 mg/L	8 mg/L	32 mg/L
Fe^{2+} concentration after addition of compound C1 (0.1M) assembling on AgNPs	**After 30 min**		
	1 mg/L	9 mg/L	22 mg/L
	After 3 h		
	1 mg/L	3 mg/L	21 mg/L
	Overnight		
	1 mg/L	3 mg/L	20 mg/L

that the removal of Fe^{2+} increased using C1 compound assembled on AgNPs and the concentration of Fe^{2+} more decreasing with time. This is related to the chelating of Fe^{2+} ions by NH group of the C1 compound and the attraction of Fe^{2+} ions due to the presence of negative charges on AgNPs.

The results for the removal of Fe^{2+} from the oil field sample are represented in Table 2 and Fig. 6. The Fe^{2+} decreased from 661 mg/L in the blank sample to 520 mg/L after 12 h with the addition of 0.1M of C1 compound assembled on AgNPs. These results indicate the ability of C1 compound assembled on AgNPs for removal of Fe^{2+} ions from the oil field sample.

4.4. Computational methodology

The structure of C1 molecule was designed and then geometrically optimized under no constraint using density function theory (DFT) with the nonlocal correlation functional B3LYP with 6-311G ++ (p,d) basis set implemented in Gaussian 09 program package, using a laptop with a processor Core i7 (8 CPU 2 GHz). E_{HOMO} and E_{LUMO} are graphically represented in Fig. 7. The following descriptors, ionization potential (I), electron affinity (A), the electronegativity (χ), global hardness (η), and softness (S), can be explained in

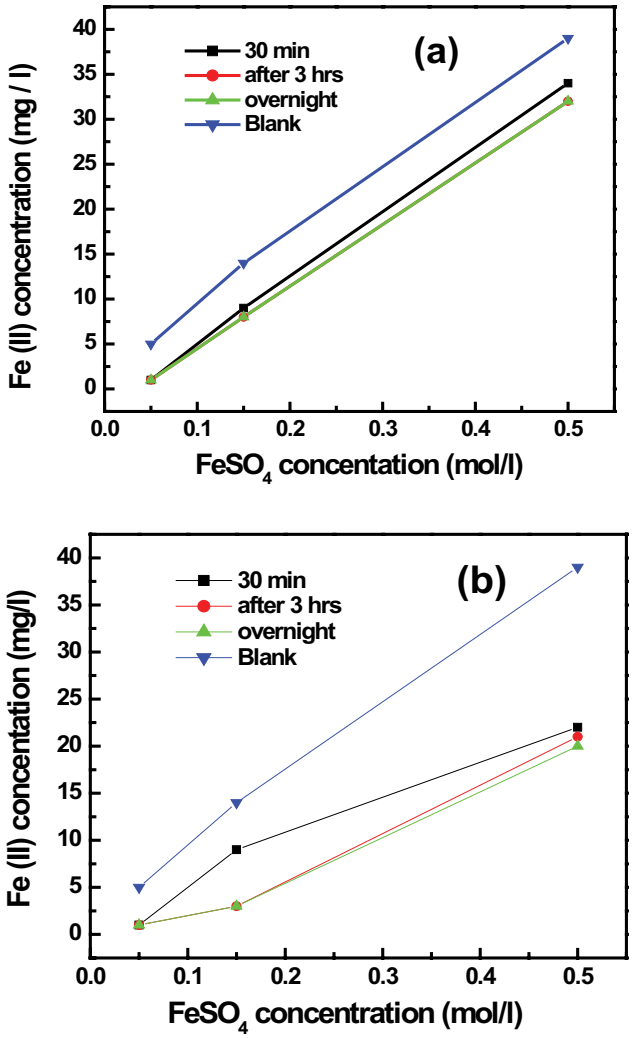

Fig. 5. Removal of Fe^{2+} using C1 compound individual (a) and with AgNPs (b).

Table 2
Removal of iron (II) from an oil field sample using the most powerful remover (C1 compound assembling on AgNPs)

Solutions	Iron (II) concentration		
Blank (standard solutions without any additions)	661 mg/L		
After addition of compound C1 (0.1M) assembling on AgNPs	**After 30 min**	**After 3 h**	**After 12 h**
	648 mg/L	644 mg/L	520 mg/L

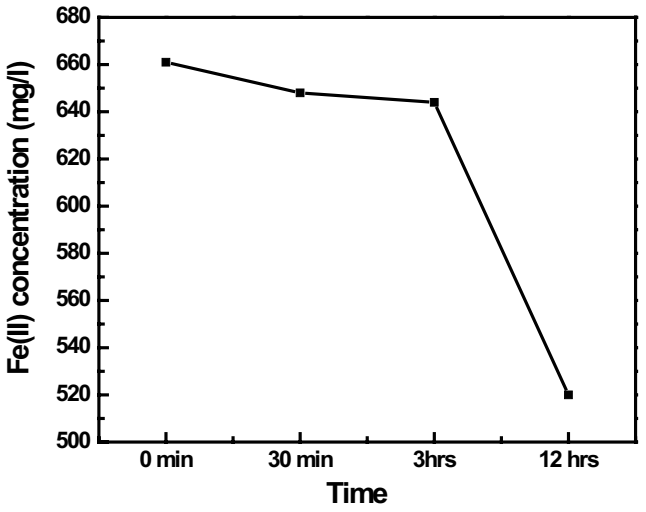

Fig. 6. Removal of Fe^{2+} from the oil field sample using the most powerful remover. (C1 compound assembling on AgNPs).

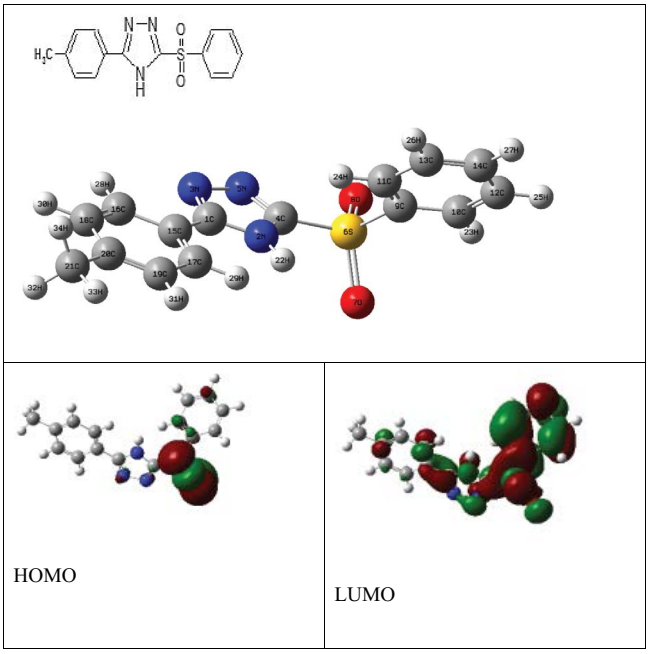

Fig. 7. Graphical representation of FMO of C1 molecule.

terms of the energy of the HOMO and the LUMO [27–29]. The electron charge distribution on the surfactant molecules was determined, which can be used to calculate Fukui indices f^+ and f^- for local nucleophilic ($f^+ = q_{N+1} - q_N$) and electrophilic attacks ($f^- = q_N - q_{N-1}$) [4]. To predict the reactive sites for electrophilic and nucleophilic attacks for the investigated molecule, molecular electrostatic potential (MEP) can discuss the reactive behavior of a wide variety of chemical systems in both electrophilic and nucleophilic reactions [30]. Occupancy of natural bond orbitals (NBOs) of C1 also explains the possible interactions between filled donor and empty acceptor NBOs, estimating their energetic importance by second-order perturbation theory.

Frontier molecule orbital density distributions of C1 molecule HOMO and LUMO are represented in Fig. 7. It shows that the electron density of HOMO appeared concentrated over SO_2 group. However, LUMO energy is distributed over the phenyl sulfonyl moiety and the 1,2,4-triazole. E_{HOMO} is likely to have a tendency of the molecule to donate electrons to an appropriate acceptor molecule of low empty molecular orbital energy [30].

The ionization energy and electron affinity can be expressed as $I = -E_{HOMO} = 0.1747$ eV and $A = -E_{LUMO} = 0.1586$ eV. The calculated energy gap is 0.0162 eV, and it is clear that the lower energy gap increases the molecular activity of the molecule. Chemical potential I is given by the following relations: $X = (I + A)/2 = 0.1666$ eV and Global hardness $\eta = (I - A)/2 = 0.0324$ eV. Parr et al. proposed the global electrophilicity power of a ligand as $x = X^2/2\eta = 4.17$ eV. As two molecules react, which one will act as an electrophile or nucleophile depends on which one has a higher (lower) electrophilicity index [31].

The local reactivity of a molecule is analyzed using the condensed Fukui indices [32], which give us information about which atoms in a molecule have a larger tendency to lose or accept an electron. Calculation of Fukui indices (f^+, f^-) for local nucleophilic and electrophilic attacks is shown in Table 3. The f^+ measures the changes of density while the molecules receive electrons and it corresponds to reactivity concerning the nucleophilic attack. As vice versa, f^- denotes the reactivity concerning electrophilic attack or when the

Table 3
Calculated Mullikan atomic charge distribution, Fukui indices of C1

Atom	N	$N+1$	$N-1$	f^+	f^-
1 C	0.336	–0.0214	0.305	–0.358	0.031
2 N	–0.687	–0.0022	–0.701	0.684	0.014
3 N	–0.309	0.0777	–0.351	0.386	0.042
4 C	0.110	0.0576	0.106	–0.053	0.005
5 N	–0.231	–0.0076	–0.277	0.223	0.046
6 S	1.173	–0.0779	1.084	–1.251	0.089
7 O	–0.520	0.2143	–0.596	0.735	0.075
8 O	–0.496	0.374	–0.570	0.870	0.074
9 C	–0.270	0.009	–0.267	0.278	–0.003
10 C	–0.075	0.002	–0.095	0.077	0.021
11 C	–0.138	–0.002	–0.154	0.136	0.017
12 C	–0.113	–0.002	–0.118	0.111	0.005
13 C	–0.102	0.002	–0.114	0.105	0.011
14 C	–0.115	0.006	–0.150	0.121	0.035
15 C	0.187	0.153	0.180	–0.034	0.007
16 C	–0.109	0.020	–0.120	0.129	0.011
17 C	–0.187	–0.011	–0.212	0.176	0.025
18 C	–0.149	–0.020	–0.164	0.129	0.015
19 C	–0.168	0.062	–0.173	0.229	0.005
20 C	0.113	0.155	0.105	0.042	0.008
21 C	–0.474	–0.007	–0.474	0.870	0.089

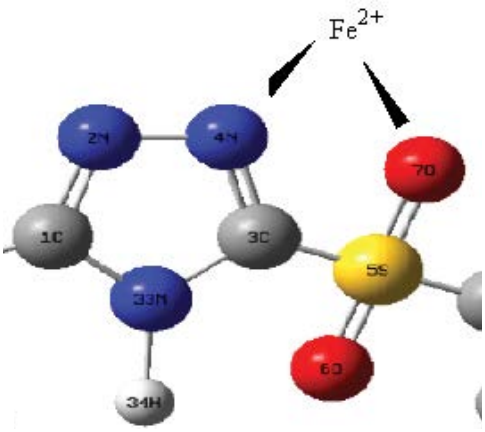

Fig. 8. Chelation of N (4) and O (7) in C1 with Fe (II).

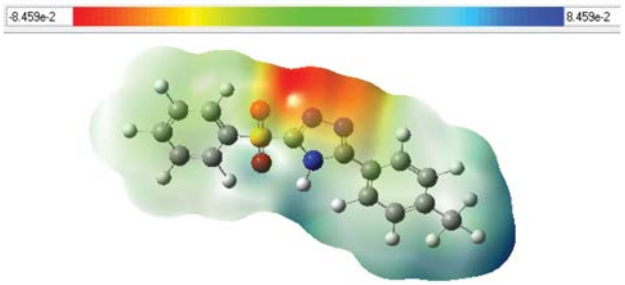

Fig. 9. MEP of 3-(p-methyl) phenyl-5-thionyl-1,2,4-triazoline (C1).

molecule loses electrons. The analysis of the local nucleophilicity indices given in Table 3 shows that the atoms labeled as C (20), O (6), O (7), N (2), and N (4) are characterized by the higher and positive values of the local nucleophilicity indices. As a result, these atoms of the given molecules are the most reactive centers, which have the most significant ability to bind to the metal surface. It can be concluded that this area is the region of reactive centers that transfers electrons from the oxygen to the Fe^{2+}. Hence, N (4) and O (7) are susceptible to chelate Fe^{2+} as shown in Fig. 8.

4.5. Molecular electrostatic potential

MEP [29] of C1 is shown in Fig. 9. Different colors represent the different values of the electrostatic potential at the surface. Potential increases in the order red < orange < yellow < green < blue. The negative (red, orange, and yellow) regions of the MEP are related to nucleophilic reactivity. The maximum negative region is localized over N (4) and O (7) in C1 and the maximum positive region is localized on the benzene ring attached to triazole moiety, indicating a possible site for nucleophilic attack. The results also prove that the susceptibility of chelation of Fe^{++} can occur via N (4) and O (7) in the title molecule.

5. Conclusion

C1 was synthesized. The nanostructure of the synthesized C1 compound was fabricated with the prepared AgNPs. The FTIR, NMR, and mass spectra analyses confirmed the chemical structure of the synthesized compound. The assembling of this compound with AgNPs was confirmed using UV and TEM analyses. The synthesized compound has high efficiency for removal of Fe^{2+} from the prepared ferrous sulfate solutions and wastewater from the oil field. The removal Fe^{2+} was improved using the nanostructure of the synthesized C1 compound with AgNPs. Quantum chemical descriptors using DFT confirmed the chelation of Fe^{2+} using the synthesized compound.

References

[1] M.M. Kamel, N.Y.M. Abdo, Synthesis of novel 1,2,4-triazoles, triazolothiadiazines, and triazolothiadiazoles as potential anticancer agents, Eur. J. Med. Chem., 86 (2014) 75–80.
[2] D. Savoia, Plant-derived antimicrobial compounds, Future Microbiol., 7 (2012) 979–990.
[3] G. Gebreyohannes, M. Gebreyohannes, Medicinal values of garlic: a review, Int. J. Med. Med. Sci., 5 (2013) 401–408.
[4] Y.M. Lee, O.C. Gweon, Y.J. Seo, J. Im, M.J. Kang, M.J. Kim, J.I. Kim, Antioxidant effect of garlic and aged black garlic in animal model of type 2 diabetes mellitus, Nutr. Res. Pract., 3 (2009) 156–161.
[5] M.H. Kim, M.J. Kim, J.H. Lee, J.I. Han, J.H. Kim, D.E. Sok, M|.R. Kim, Hepatoprotective effect of aged black garlic on chronic alcohol-induced liver injury in rats, J. Med. Food, 14 (2011) 732–738.
[6] P. Domenico, R.J. Salo, S.G. Novick, P.E. Schoch, K. Van Horn, B.A. Cunha, Enhancement of bismuth antibacterial activity with lipophilic thiol chelators, Antimicrob. Agents Chemother., 41 (1997) 1697–1703.
[7] D. Tenkrat, T. Hlincik, O. Prokes, Natural gas odorization, Natural Gas, InTech, Institute of Chemical Technology Prague, Czech Republic, 2010.
[8] F. Ke, J. Jiang, Y. Li, J. Liang, X. Wan, S. Ko, Highly selective removal of Hg^{2+} and Pb^{2+} by thiol-functionalized Fe_3O_4@ metal-organic framework core-shell magnetic microspheres, Appl. Surf. Sci., 413 (2017) 266–274.
[9] F.A. Hassan, K.W. Younus, Biological evaluation of some azole derivatives in cooling fluids (lubricant oils), Res. J. Biol. Sci., 7 (2012) 48–51.
[10] S.P. Pardeshi, S.V. Patil, R. Patil, V.D. Bobade, Synthesis and antimicrobial activities of some 1,2,4- triazolo[3,4-b][1,3,4] thiadiazoles and 1,2,4-triazolo [3,4-b][1,3,4]thiadiazines bearing bistrifluoromethyl phenyl moiety, J. Chem. Pharm. Res., 6 (2014) 675–681.
[11] A.J.Kh. Atia, S.S. Al-Mufrgeiy, Synyhesis and antibacterial activities of new 3-amino-2-methylquinazolin-4(3H)-one derivatives, Am. J. Chem., 2 (2012) 150–156.
[12] T. Taj, R.R. Kamble, T. Gireesh, B.V. Badami, An expeditious green synthesis of Schiff bases and azetidinones derivatised with 1,2,4-triazoles, J. Chem. Sci., 123 (2011) 657–666.
[13] O. Bekircan, E. Menteşe, S. Ülker, C. Kucuk, Synthesis of some new 1,2,4-triazole derivatives starting from 3-(4-chlorophenyl)-5-(4-methoxybenzyl)-4H-1,2,4-triazol with anti-lipase and anti-urease activities, Arch. Pharm. Chem. Life Sci., 347 (2014) 387–397.
[14] H.M. Abdullah, I.K. Jassim, M.N. Safi, Synthesis and characterization of new heterocyclic compounds with studying its biological activity, Karbala J. Pharm. Sci., 4 (2012) 115–135.
[15] S. Sripriya, C. Subha, A. Selvaraj, The inhibition chemistry of 2-amino, 5-phenyl 1, 3, 4-triazole for aluminium in hydrochloric acid solution, IOSR J. Appl. Chem., 6 (2013) 25–29.
[16] J.C. Er, M.K. Tang, C.G. Chia, H. Liew, M. Vendrell, Y.T. Chang, Megastokes BODIPY-triazoles as environmentally sensitive turn-on fluorescent dyes, J. Chem. Sci., 4 (2014) 2168–2176.
[17] V.N. Bulut, C. Duran, A. Gundogdu, M. Soylak, N. Yildirim, M. Tufekci, Triazole derivatives as a new acid-base indicator, Bull. Chem. Soc. Ethiop., 24 (2010) 457–460.

[18] S. Cassani, S. Kovarich, P.P. Roy, L. Van der Wal, P. Gramatica, Daphnia and fish toxicity of (benzo)triazoles: validated QSAR models, and interspecies quantitative activity-activity modeling, J. Hazard. Mater., 258–259 (2013) 50–60.
[19] M. Lamann, L. Leiton, I.N. Vega, B.L. Rivas, N. D'Accorso, New copolymers with triazole pendant groups: synthesis, characterization and their application to remove heavy metals, Adv. Mater. Sci., 2 (2017) 1–6.
[20] S. Kotthaus, B.H. Gunther, R. Hang, H. Schafer, Study of isotropically conductive bondings filled with aggregates of nano-sited Ag-particles, IEEE Trans. Compon. Packag. Technol. Part A., 20 (1997) 15–20.
[21] G. Cao, Nanostructures and Nanomaterials: Synthesis, Properties and Applications, Imperial College Press, London, UK, 2004.
[22] J. Bernstein, H.L. Yale, K. Losee, M. Holsing, J. Martins, W.A. Lott, The chemotherapy of experimental tuberculosis. III. The synthesis of thiosemicarbazones and related compounds, J. Am. Chem. Soc., 73 (1951) 906–912.
[23] K. Bahrami, M.M. Khodaei, M. Soheilizad, Direct conversion of thiols to sulfonyl chlorides and sulfonamides, J. Org. Chem., 74 (2009) 9287–9291.
[24] N.A. Abdel-Latif, T.H. El-Shihi, I.E. Islam, E.R. El-Sawy, Synthesis of some new indole derivatives incorporated to heterocyclic systems and evaluation of their antimicrobial activity, Egypt. Pharm. J. (NRC), 4 (2005) 313–329.
[25] H.H.H. Hefni, E.M. Azzam, E.A. Badr, M. Hussein, S.M. Tawfik, Synthesis, characterization and anticorrosion potentials of chitosan-g-PEG assembled on silver nanoparticles, Int. J. Biol. Macromol., 83 (2016) 297–305.
[26] E.M.S. Azzam, Gh. Eshaq, A.M. Rabie, A.A. Bakr, A.A. Abd-Elaal, A.E. El Metwally, S.M. Tawfik, Preparation and characterization of chitosan-clay nanocomposites for the removal of Cu (II) from aqueous solution, Int. J. Biol. Macromol., 89 (2016) 507–517.
[27] J.H. Al-fahemi, M. Abdallah, E.A.M. Gad, B.A.A.L. Jahdaly, Experimental and theoretical approach studies for melatonin drug as safely corrosion inhibitors for carbon steel using DFT, J. Mol. Liq., 222 (2016) 1157–1163.
[28] E.A.M. Gad, E.M.S. Azzam, S.A. Halim, Theoretical approach for the performance of 4-mercapto-1-alkylpyridin-1-ium bromide as corrosion inhibitors using DFT, Egypt. J. Pet., (2017) 6–10 (In press).
[29] C.Y. Panicker, H.T. Varghese, P.S. Manjula, B.K. Sarojini, B. Narayana, J.A. War, S.K. Srivastava, C.V. Alsenoy, A.A. Al-Saadi, FT-IR, HOMO-LUMO, NBO, MEP analysis and molecular docking study of 3-Methyl-4-{(E)-[4-(methylsulfanyl)-benzylidene]amino}1H-1,2,4-triazole-5(4H)-thione, Spectrochim. Acta A Mol. Biomol. Spectrosc., 151 (2015) 198–207.
[30] K. Laarej, M. Bouachrine, S. Radi, S. Kertit, B. Hammouti, Quantum chemical studies on the inhibiting effect of bipyrazoles on steel corrosion in HCl, J. Chem., 7 (2010) 419–424.
[31] R.G. Parr, L.V. Szentpály, S. Liu, Electrophilicity index, J. Am. Chem. Soc., 121 (1999) 1922–1924.
[32] A.A. Siaka, N.O. Eddy, S.O. Idris, L. Magaji, Experimental and computational study of corrosion potentials of penicillin G., Res. J. Appl. Sci., 6 (2011) 487–493.

Supplementary Information

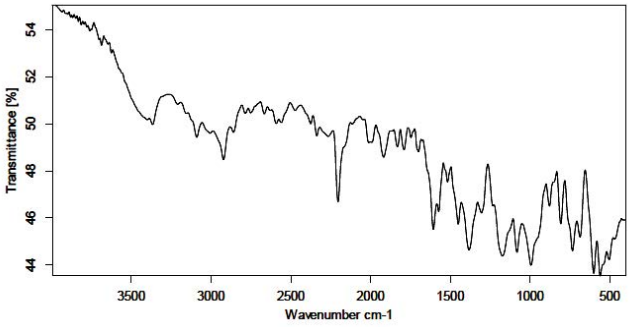

Fig. S1. FTIR of the synthesized C1 compound.

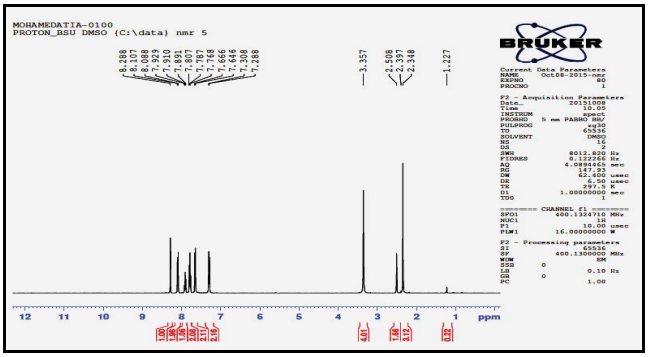

Fig. S2. ^{1}HNMR of the synthesized C1 compound.

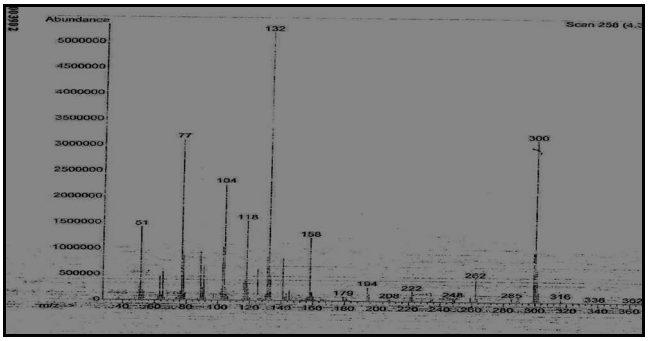

Fig. S3. Mass spectra of the synthesized C1 compound.

Author Query: